
Self-Conditioned Denoising for Atomistic Representation Learning

Tynan J. Perez¹ Rafael Gómez-Bombarelli²

Abstract

The success of large-scale pretraining in NLP and computer vision has catalyzed growing efforts to develop analogous foundation models for the physical sciences. However, pretraining strategies using atomistic data remain underexplored. To date, large-scale supervised pretraining on DFT force-energy labels has provided the strongest performance gains to downstream property prediction, out-performing existing methods of self-supervised learning (SSL) which remain limited to ground-state geometries, and/or single domains of atomistic data. We address these shortcomings with Self-Conditioned Denoising (SCD), a backbone-agnostic reconstruction objective that utilizes self-embeddings for conditional denoising across any domain of atomistic data, including small molecules, proteins, periodic materials, and 'non-equilibrium' geometries. When controlled for backbone architecture and pre-training dataset, SCD significantly outperforms previous SSL methods on downstream benchmarks and matches or exceeds the performance of supervised force-energy pretraining. We show that a small, fast GNN pretrained by SCD can achieve competitive or superior performance to larger models pretrained on significantly larger labeled or unlabeled datasets, across tasks in multiple domains. Our code is available at: <https://github.com/TyJPerez/SelfConditionedDenoisingAtoms>

1. Introduction

The development of 'foundation models' has transformed natural language processing (NLP) and computer vision. The prevailing training paradigm now employs a two-stage

process: pretraining on large unlabeled datasets to learn generalizable representations, followed by fine-tuning on smaller, labeled datasets for specialized tasks. The success of large-scale pretraining has motivated the development of analogous foundation models in atomistic sciences, including chemistry, structural biology, and materials science (Yuan et al., 2025; Zhang et al., 2025). These efforts are driven by their potential for accelerated atomistic simulation, direct structure-to-property prediction, and inverse design—capabilities that could significantly accelerate the discovery of new drugs and materials.

In chemistry and materials science, the most notable progress toward this vision has come from researchers developing machine-learned interatomic potentials (MLIPs) to accelerate atomistic simulation. Pretrained MLIPs - such as UMA(Wood et al., 2025), MACE(Batatia et al., 2025) and Orb(Rhodes et al., 2025) - have achieved remarkable accuracy in DFT force-energy predictions by supervised pretraining on large, diverse atomistic datasets. These models have enabled near-DFT quality simulations and structural relaxations at speeds and scales far exceeding those of traditional DFT. While often termed 'foundation models' (or more appropriately 'foundation potentials'), they differ from their counterparts in NLP and CV in one key regard: current foundation potentials are pretrained exclusively via supervised learning on precomputed forces and energies. However, scaling supervised pretraining with DFT labels is computationally expensive; generating forces and energies for the 100M geometries in the OMol25 dataset required six billion CPU core-hours (Levine et al., 2025).

In other fields, foundation models typically rely on self-supervised learning (SSL) objectives that leverage vast, unlabeled datasets. However, unlike images and text, which are often collected without labels, atomistic datasets are typically generated via computational methods (such as DFT) that inherently produce force and energy labels as part of the data generation process. Although force and energy values vary depending on the DFT functional used, prior work has overcome this by using multiple prediction heads and demonstrating clear benefits to supervised pretraining on large, diverse datasets containing labels derived from multiple functionals (Wood et al., 2025; Shoghi et al., 2023). Consequently, supervised pretraining with DFT labels remains the dominant paradigm, outperforming existing SSL

¹Department of Chemistry, Massachusetts Institute of Technology, 77 Massachusetts Avenue, Cambridge, 02139, MA, USA

²Department of Materials Science and Engineering, Massachusetts Institute of Technology, 77 Massachusetts Avenue, Cambridge, 02139, MA, USA. Correspondence to: Rafael Gómez-Bombarelli <rafagb@mit.edu>.

methods on simulation and property prediction benchmarks (Shoghi et al., 2023; Zaidi et al., 2022). However, the ratio of 'ground-truth' DFT labeled atomistic data is likely to change as more atomistic geometries are produced using MLIP-driven simulation or relaxation, and generative models (Wohlwend et al., 2025; Passaro et al., 2025; Lemos et al., 2025; Wood et al., 2025; Zeni et al., 2023; Batatia et al., 2025; Li et al., 2024). Nevertheless, adapting SSL methods from other fields has remained a challenge due to the unique attributes of 3D atomistic data. Atomistic data has no fixed size (samples range from 3 to over 3000 atoms), samples may exhibit periodicity in 3D space, and learned representations must be sensitive to small changes in atomic position to achieve accurate predictions in geometrically sensitive tasks (structural relaxation, simulation, binding affinity predictions, etc).

Previous work in computer vision suggests that self-supervised pretraining can yield more interpretable and generalizable representations than supervised learning (Chen et al., 2021; Oquab et al., 2024; Siméoni et al., 2025), achieving performance competitive with supervised models even on identical datasets (He et al., 2021; Tomasev et al., 2022). This is because supervised learning only requires a model to represent features of the training data that are relevant to a specific task, becoming invariant to uncorrelated features. In contrast, generative SSL encourages a model to represent the full feature distribution within a training dataset, often producing internal representations with superior transferability. In this work, we demonstrate that this principle holds for 3D atomistic data as well.

2. Background

2.1. Contrastive Learning on Low Dimensional Representation

Early atomistic SSL relied on maximizing mutual information between 3D geometries and lower-dimensional representations, such as 2D graphs or SMILES (Liu et al., 2022; Stärk et al., 2022; Hu et al., 2020). While these methods improved performance for predictions on lower dimensional inputs, they often underperformed supervised models acting on 3D inputs, and were not applicable in configurationally aware tasks like force prediction or ligand docking. Furthermore, multi-modal contrastive approaches are inapplicable to systems lacking 1D representations, such as periodic crystals, limiting their generality.

2.2. Node Denoising

Node denoising pretraining emerged as a more generalizable alternative, operating directly on 3D point clouds. Formally, given an input structure with N atoms $\mathbf{x} \in \mathbb{R}^{N \times 3}$, we sample Gaussian noise $\boldsymbol{\varepsilon} \sim \mathcal{N}(\mathbf{0}, \sigma^2 \mathbf{I})$ to generate a corrupted

geometry $\tilde{\mathbf{x}} = \mathbf{x} + \boldsymbol{\varepsilon}$. A neural network ϕ_θ is then trained to predict the noise vector on each atom of the corrupted geometry:

$$\mathcal{L}_{\text{denoise}} = \mathbb{E}_{\mathbf{x}, \boldsymbol{\varepsilon}} \left[\|\phi_\theta(\tilde{\mathbf{x}}) - \boldsymbol{\varepsilon}\|_2^2 \right] \quad (1)$$

Unlike contrastive objectives that promote multi-view invariance, noise prediction encourages equivariance to geometric perturbations, making it effective for learning geometric features of local atomic environments. Pretraining by node denoising has proven useful as both an auxiliary loss (Godwin et al., 2022; Liao & Smidt, 2022; Liao et al., 2023) and a standalone pretraining task (Zaidi et al., 2022; Liu et al., 2023; Fang et al., 2025; Jiao et al., 2025).

2.3. State of The Art Pretraining

Despite its elegance and generality, standard node denoising struggles to match the efficacy of supervised force-energy (FE) pretraining, largely because it fails to benefit from training on non-ground state ('non-equilibrium') geometries (Feng et al., 2023). Early interpretations suggested that denoising approximates learning a 'near-equilibrium' force field (Zaidi et al., 2022). However, for high-energy configurations, noise vectors $\boldsymbol{\varepsilon}$ (the vectors pointing from corrupted atom positions to uncorrupted positions) are unlikely to resemble true forces and the difference between a corrupted input and a valid non-corrupted higher-energy configuration becomes ambiguous. This makes denoising 'non-equilibrium' geometries an ill-posed task without additional information. One solution is to incorporate a force encoding (Liao et al., 2024), but this is no longer SSL as it requires force-energy labels.

Others have shown that there is little correlation between noise vectors and true DFT forces even for ground-state geometries (Ni et al., 2023). Variations on the node denoising objective have improved performance, but at the cost of introducing domain-specific constraints, such as torsional noise in *Frad* (Ni et al., 2024), or pseudo-force targets in *SliDe* (Ni et al., 2023). Others have explored specialized masking, block-wise denoising, hybrid contrastive objectives with lower-dimensional representations, and scaling pretraining on larger datasets with up to 200M geometries (Fang et al., 2025; Feng et al., 2024; Jiao et al., 2025; Zhou et al., 2023). However, these approaches often sacrifice generality and remain limited to ground state geometries of small molecules. To date, general-purpose SSL objectives have not matched the performance of supervised FE pretraining on downstream property prediction tasks (Shoghi et al., 2023; Kim et al., 2025).

3. Method

3.1. The Limitations of Node Denoising

We identify three critical limitations of standard node denoising as a pretraining objective:

(s1) Locality of Node Denoising: GNNs often struggle with global representations and long-range correlations. Node denoising fails to produce strong global semantic learning because: (1) Gaussian noise applied to atom positions lacks long-range correlation across space, and (2) small perturbations in atom position can be estimated with high accuracy using a relatively small, local context window.

(s2) Scalar vs. Vector Embedding Pressure:

Equivariant GNNs commonly partition node embeddings into multiple channels determined by rotational symmetry groups ($L = 0, 1, 2, \dots$). Because noise prediction is an equivariant vector ($L = 1$) objective, it primarily impacts $L = 1$ channels. While denoising gradients propagate through all model parameters, there is insufficient pressure on invariant scalar embeddings ($L = 0$) to develop good semantic representations. This is problematic for downstream property predictions, which are often roto-translation invariant and rely on the invariant ($L = 0$) channel.

(s3) Ambiguity with Non-Equilibrium Structures:

Standard node denoising pretraining does not benefit from including 'non-equilibrium' or high-energy geometries. Without additional context, models cannot distinguish between a corrupted input geometry and a valid, high-energy target geometry. This creates ambiguity in the objective when training on datasets that include non-ground-state conformers.

3.2. Self-Conditioned Denoising

Self-Conditioned Denoising (SCD) addresses all three shortcomings of the standard denoising objective by incorporating a conditional embedding in the model architecture as shown in eqn. 2:

$$\mathbb{E}_{q_\sigma(\tilde{\mathbf{x}}, \mathbf{x})} \left[\|\phi_\theta(\tilde{\mathbf{x}}|\mathbf{c}) - \varepsilon\|_2^2 \right], \quad \mathbf{c} = f_\eta(\mathbf{x}) \quad (2)$$

Here, $c \in \mathbb{R}^d$ is an embedding vector that represents the uncorrupted target geometry. This conditioning provides the model with enough information to distinguish between corrupted samples and a valid target conformation (addressing s3). The conditional embedding itself can then be used as a training objective to develop meaningful invariant (L0) representation (addressing s2). This in turn pushes the embedding model (f_η) to develop better global/semantic representation (addressing s1). In SCD, we use the same model

Algorithm 1 SCD Pretraining and Fine-tuning Pipeline

Require: Dataset \mathcal{D} , noise scales $\sigma_{\text{corr}}, \sigma_{\text{reg}}$, model ϕ_θ

Ensure: Trained parameters θ

```

1: Pretraining
2: for each minibatch  $\mathbf{x} \sim \mathcal{D}$  do
3:    $(\mathbf{x}, \tilde{\mathbf{x}}, \varepsilon) \leftarrow \text{CORRUPT}(\mathbf{x}, \sigma_{\text{corr}}, \sigma_{\text{reg}}) \triangleright$  create views
4:    $(\mathbf{c}_{L0}, \mathbf{v}_{L1}, \mathbf{y}_{L0}) \leftarrow \phi_\theta(\mathbf{x}) \triangleright$  self-embedding
5:    $(\tilde{\mathbf{c}}_{L0}, \tilde{\mathbf{v}}_{L1}, \tilde{\mathbf{y}}_{L0}) \leftarrow \phi_\theta(\tilde{\mathbf{x}}, \mathbf{c}_{L0}) \triangleright$  conditional denoising
6:    $\mathcal{L}_{\text{pre}} \leftarrow \text{MSE}(\tilde{\mathbf{v}}_{L1}, \varepsilon)$ 
7:    $\theta \leftarrow \theta - \eta \nabla_\theta \mathcal{L}_{\text{pre}}$ 
8: end for

9: Fine-tuning / Inference
10: for each labeled sample  $(\mathbf{x}, \mathbf{y})$  do
11:    $(\mathbf{c}_{L0}, \mathbf{v}_{L1}, \mathbf{y}_{L0}) \leftarrow \phi_\theta(\mathbf{x})$ 
12:    $\mathcal{L}_{\text{fine}} \leftarrow \text{loss}(\mathbf{y}_{L0}, \mathbf{y})$ 
13:    $\theta \leftarrow \theta - \eta \nabla_\theta \mathcal{L}_{\text{fine}}$ 
14: end for
    
```

as both the embedding model f_η , and the noise predictor, ϕ_θ , during each optimizer step of pretraining (shown in eqn 3).

$$\begin{aligned} & \mathbb{E}_{q_\sigma(\tilde{\mathbf{x}}, \mathbf{x})} \left[\|\phi_\theta(\tilde{\mathbf{x}}|\mathbf{c}) - \varepsilon\|_2^2 \right] \\ &= \mathbb{E}_{q_\sigma(\tilde{\mathbf{x}}, \mathbf{x})} \left[\|\phi_\theta(\tilde{\mathbf{x}}|\phi_\theta(\mathbf{x})_{L0})_{L1} - \varepsilon\|_2^2 \right] \quad (3) \end{aligned}$$

$$\mathbf{c} = \phi_\theta(\mathbf{x})_{L0} \in \mathbb{R}^d, \quad \phi_\theta(\tilde{\mathbf{x}}|\mathbf{c})_{L1} \in \mathbb{R}^{N \times 3}$$

Implementation of the SCD objective is summarized by algorithm 1 and visualized in figure 1. First a forward pass is made using uncorrupted geometries (\mathbf{x}). The resulting invariant (L0) embeddings are sum-pooled across nodes and passed through a two-layer MLP embedding head, forming a single embedding per geometry. This creates an information bottleneck that encourages semantic representation. The embedding is then used as conditional guidance for a second forward pass during which a corrupted geometry ($\tilde{\mathbf{x}}$) is used as input. The L1 equivariant output from the second pass is then used to predict the per-node noise corruption. To preserve unconditional behavior, we drop 20% of conditional embeddings each pass. After pretraining is complete, downstream supervised finetuning and inference only requires a single model pass without conditioning.

3.3. Backbone Architectures

Following established baselines, we implement SCD using TorchMD-Net (also known as Equivariant Transformer or *ET*) as the primary backbone (Thölke & Fabritius, 2022; Ni et al., 2024; 2023; Feng et al., 2024; Zaidi et al., 2022). To ensure a fair comparison, all models we train use an embedding dimension of 256, 8 layers, and 8 heads, consistent

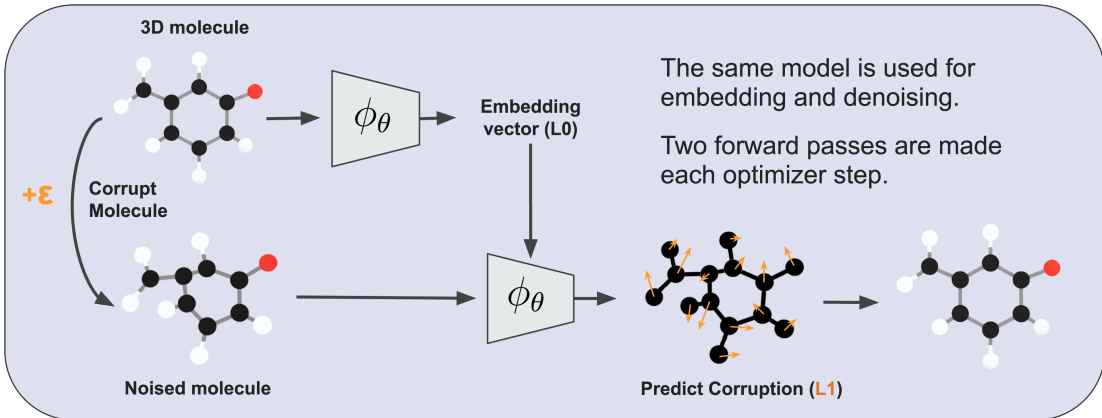


Figure 1. Self-Conditioned Denoising Pretraining

with previous SSL studies (see Table 10).

The ET backbone architecture is a lightweight, attention-based GNN that lacks both tensor products and angular embeddings that are now commonly found in equivariant MLIPs. However, other denoising variations like *Frad* (Ni et al., 2024) and *SliDe* (Ni et al., 2023) require explicit angular information and utilize a modified “Geometric Equivariant Transformer” (GET). To achieve a direct comparison with these methods, we evaluate SCD on both the standard ET and the more expressive GET backbones.

To incorporate conditional inputs into these non-conditional backbones, we replace existing pre-attention layer normalization with Adaptive Layer Normalization (*AdaNorm*), analogous to its use in Diffusion Transformers (Peebles & Xie, 2023). We find that *AdaNorm* has a negligible impact on inference speed or memory overhead. In contrast, the GET backbone is approximately $4\times$ slower and has twice as many parameters as the ET backbone. We denote the conditional versions of these two architectures as **CT** (Conditional TorchMD-Net) and **CGT** (Conditional Geometric TorchMD-Net), respectively. Additional implementation details and speed comparisons are provided in Appendix B.

3.4. Datasets

Atomistic model training has often been siloed to single domains, typically focusing on small molecules, bio-molecules, or periodic materials independently. Although recent works have trained or pretrained on increasingly diverse datasets (Fang et al., 2025; Joshi et al., 2025; Shoghi et al., 2023), multi-domain pretraining remains logistically challenging and under-explored. In this work, we evaluate models pretrained on a range of single domain datasets, with varying conformational diversity, as well as a combined multi-domain aggregate dataset (see Table 1). All pretrained models are benchmarked on three representative tasks: 1) QM9 HOMO energy for small molecules (Ramakrishnan

et al., 2014), 2) Matbench band gap for periodic materials (Dunn et al., 2020), and 3) Ligand Binding Affinity (LBA) for bio-molecules (Townshend et al., 2022). Dataset descriptions are provided in Appendix D.

4. Results

4.1. SCD Outperforms Other SSL Methods on Atomistic Data

Given the same pretraining dataset and backbone architecture, SCD pretraining significantly outperforms other forms of node denoising. When compared to standard node denoising pretraining (aka ‘coord’) we find that SCD conveys large improvements (19.6-45.5%) across all QM9 targets tested, except heat capacity (C_v) (-5%) (see table 2). In table 3 we compare SCD against SOTA methods *Frad* and *Slide*. We find that SCD pretraining, with either backbone architecture (CT or CGT) outperforms prior methods on most QM9 targets. Table 15 in the Appendix provides an additional comparison between our SCD pretrained models and other methods that used different backbone architectures and/or different pretraining datasets.

4.2. SCD Benefits From Pretraining on Any Atomistic Data Source

Making use of all available atomistic data during pretraining remains a notable bottleneck in scaling the atomistic foundation models. Prior SSL work has been limited to ground-state geometries of small molecules (Ni et al., 2024; 2023; Feng et al., 2024), while force-energy pretraining across datasets from different DFT functionals often requires the use of dataset specific heads or other specialize architecture components (Shoghi et al., 2023; Wood et al., 2025). In this work, we find that SCD pretraining derived a significant benefit from every dataset tested. In Table 4 we show how datasets from different domains, and conformational diversity, impact QM9 homo energy prediction

Table 1. Summary of Pretraining and Benchmarking Datasets

Pretraining Dataset	Domain	Unique Structures	Total Geometries	Origin/functional
PCQ (PCQM4Mv2)	Small Molecules	3.378M	3.378M	B3LYP/6-31G* DFT
GEOM10	Small Molecules	304,339	2.7M	GFN2-xTB , conformers
AMP20 (Alex-MP-20)	Periodic Materials	607,673	607,673	PBEsol DFT
SAIR	Protein-Ligand	888k	4.4M	Boltz-1x, conformers
ALL (AllAtoms)	Above, mixed	5.2M	11.3M	PCQ, GEOM10, AMP20, SAIR
OMol25 (4M split)	mixed organic molecules	—	4M	MD, Non-equilibrium
Benchmarking Dataset	Domain	Training Set Geometries	Task	
QM9	Small Molecules	110k	properties computed from DFT	
Matbench (mp gap)	Periodic Materials	85k	band gap energy computed from DFT	
LBA	Protein-Ligand	4k	ligand binding affinity ($-\log(K_d)$)	

PCQ(Nakata & Shimazaki, 2017), GEOM(Axelrod & Gomez-Bombarelli, 2022), AMP20(Jain et al., 2013; Schmidt et al., 2023; 2022), SAIR (Lemos et al., 2025), OMol25(Levine et al., 2025), Boltz-1x (Wohlwend et al., 2025), QM9(Ramakrishnan et al., 2014), Matbench(Dunn et al., 2020), LBA(Townshend et al., 2022)

Table 2. **SCD vs. Standard Node Denoising.** Given the same backbone and pretraining datasets (PCQ), SCD significantly outperforms standard denoising (*Coord*). Best results are **bolded**. All values reported as MAE on the test set.

Method	Baseline	Coord	SCD	% imp.
Backbone	ET	ET	CT	vs. Coord
HOMO (meV)	20.3	17.7	12.7	28.2%
LUMO (meV)	17.5	14.3	11.5	19.6%
Gap (meV)	36.1	31.8	24.5	23.0%
ZPVE (meV)	1.84	1.71	1.18	21.0%
U_0 (meV)	6.15	6.57	3.58	45.5%
U (meV)	6.38	6.11	3.50	42.7%
H (meV)	6.16	6.45	3.52	45.4%
G (meV)	7.62	6.91	5.29	23.4%
α (a_0^3)	0.059	0.0517	0.0377	27.1%
C_v (cal/molK)	0.026	0.020	0.021	-5.0%

error. Here, we report that SCD pretraining benefits from including both multiple conformers (GEOM1 vs GEOM10), and non-equilibrium structures (i.e. OMol25). We also find that large datasets are not necessarily required to see a significant benefit from SCD pretraining. Pretraining on a random 10% subset of PCQ (300k samples) provided only slightly lower performance than pretraining on the whole dataset (3.4M samples). Overall, we find that the most significant predictor of downstream prediction accuracy is the similarity between the pretraining dataset and the finetuning dataset.

4.3. Better Models Have Smoother Latent Spaces

Figure 2 provides UMAPs for QM9 molecule embeddings from both untrained and pretrained models, colored by the number of atoms in each sample (N). We observe that an untrained ET model has a strong bias towards highly clustered, extensive representations - mean pooled atom embeddings that are highly correlated with the number of atoms in each

Table 3. **SCD vs. Variations on Node Denoising.** All models are pretrained on PCQ. Percent improvement (% imp.) is calculated between SliDe and SCD pretraining with the most similar backbone, CGT. **Bold** denotes best; underline denotes second best. All values reported as MAE on the test set.

Method	Frad	SliDe	SCD	SCD	% imp.
Backbone	GET	GET	CT	CGT	vs. SliDe
HOMO (meV)	15.2	13.6	<u>12.7</u>	9.65	29.0%
LUMO (meV)	13.7	12.3	<u>11.5</u>	9.05	26.4%
Gap (meV)	27.8	26.2	<u>24.5</u>	19.7	24.8%
ZPVE (meV)	1.42	1.52	1.18	<u>1.22</u>	19.8%
U_0 (meV)	5.33	4.28	3.58	<u>3.97</u>	8.1%
U (meV)	5.62	4.29	3.50	<u>4.11</u>	4.4%
H (meV)	5.55	4.26	3.52	<u>4.00</u>	6.5%
G (meV)	6.19	5.37	5.29	<u>5.29</u>	1.5%
α (a_0^3)	<u>0.0374</u>	0.0366	0.0377	0.0383	-4.6%
C_v (cal/molK)	0.020	0.019	0.021	0.019	0.0%

molecule. We find that standard node denoising ('coord') results in a smooth but highly extensive representation space (this was also observed by (Li et al., 2024)). We believe this is a consequence of features that are too biased towards local node geometry, rather than global semantic representation (non-extensive features). In models pretrained by SCD, we observe greater smoothing and a reduced correlation with N, suggesting a more semantic representation. Empirically, we find models with a smoother, less extensive, embedding space reach a lower prediction error on QM9 targets. Additional plots are provided in figure 4.

4.4. Comparing SCD Models with other Pretrained Models

In table 5, we show that pretraining and finetuning a simple, fast GNN with SCD is more cost effective than supervised training from scratch with more advanced tensor-product based architectures like Equiformer(Liao et al., 2023), yet it

Table 4. **SCD Pretraining on Diverse Data Sources.** SCD enables effective pretraining across ground-state and non-equilibrium conformers from varied sources. Every pretraining configuration tested shows improvement over the non-pretrained baseline.

Pretraining Dataset	Source / Quality	Unique Mol.	Total Geom.	QM9 HOMO (MAE, meV)
baseline				20.3
PCQ	DFT (B3LYP/6-31G*)	3,378,606	3,378,606	12.7
PCQ-300k	DFT (B3LYP/6-31G*)	300,000	300,000	13.0
GEOM10	xTB (Conformers)	304,339	2,791,929	13.2
GEOM1	xTB (Lowest Energy)	304,339	304,339	13.7
AMP20	DFT (PBEsol)	675,204	675,204	14.6
SAIR	Boltz-1 (Synthetic Conformers)	888,104	4.4M	14.6
SAIR-Pocket	Boltz-1 (Synthetic Conformers)	888,104	4.4M	14.5
ALL	Mixed Aggregate	5,246,253	11.3M	12.7
OMol25 ¹	Non-equilibrium (MD)	—	3,986,754	12.8

¹ The number of unique molecules in the OMol25 4M split is not reported (Levine et al., 2025).

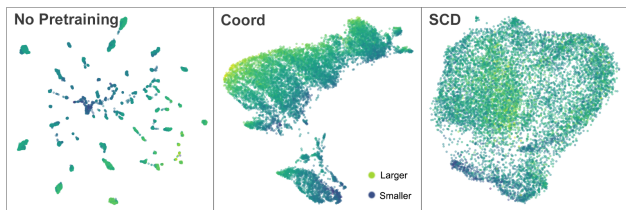


Figure 2. **UMAP of molecule embeddings colored by atom count:** SCD results in smoother, less extensive, semantically rich representation. 'Coord' refers to standard node denoising pretraining. See figure 4 for additional plots and details.

provides downstream results that are comparable to larger models pretrained by supervised force-energy prediction using orders of magnitude more data (Shoghi et al., 2023).

SCD pretrained models also deliver strong results in property prediction for materials and proteins. In table 6 we show that our 10M parameter model pretrained on 675k periodic materials can achieve similar accuracy in bandgap prediction (within 2%) as a 27M parameter model trained on 120M force-energy labeled geometries (108M of which are materials geometries). Table 7 presents a similar outcome for predictions of ligand binding affinity (LBA) on protein-ligand complexes. In this case, we can adjust the SCD objective to take advantage of an existing conditional relationship in the data: bound ligand conformation is determined by pocket geometry. We find that pretraining with 'pocket conditional ligand denoising' (CT-SCD-SAIR-Pocket) conveys an additional task specific benefit, and achieves state of the art results (See appendix section C.1.1 for more details).

In order to make a direct comparison between SCD and force-energy pretraining, we also benchmark a force-energy pretrained CT model using the 4M split of OMol25, and compare it with a CT model pretrained using SCD on the exact same geometries (without force-energy labels). We summarize these results in Table 8, and show that SCD

pretraining performs roughly as well (-1.1%) or slightly better (+3.9%) than force-energy pretraining across all three tasks.

4.5. Conclusion

In this work, we present a limited exploration of the SCD pretraining objective across multiple domains of pretraining data and property prediction tasks. We find that SCD pretraining provides robust improvements on all tasks investigated and matches or outperforms the benefits of force-energy pretraining, as well as other pretraining methods. Small SCD pretrained models achieve state-of-the-art results across multiple domains: QM9, Matbench properties, and Ligand binding affinity benchmarks. Overall, our findings can be summarized through several key observations:

All data is useful for pretraining: We observed that SCD pretraining on atomistic data from any domain or source (DFT accurate ground-state, 'non-equilibrium', or diffusion-generated) conveyed an improvement across all benchmarking tasks. Surprisingly, we find that even ligand binding affinity predictions are improved when pretraining on periodic materials (+12%), and pretraining with non-periodic, non-equilibrium molecule geometries (OMol25) conveyed a surprising benefit to bandgap predictions in periodic materials (+26.9%) (see Table 8). However, we hypothesize that at least some of these benefits may stem from pre-smoothing of the representation space prior to task-specific fine-tuning (Figure 4).

Pretraining is not necessarily expensive: Our backbone architecture is neither complex nor state-of-the-art, and without pretraining, it provides only a modest baseline. However, we find that a simple, fast GNN pretrained by SCD can outperform supervised learning with advanced tensor-product based architectures (e.g., EquiformerV2 (Liao et al., 2023)) in both prediction accuracy and total compute cost (includ-

Self-Conditioned Denoising for Atomistic Representation Learning

Table 5. Comparing Computational Costs and Performance. SCD pretraining enables competitive performance at a lower cost than more advanced Clebsch-Gordan tensor product based architectures, and large-scale force-energy (FE) pretrained models. **Bold** denotes best; underline denotes second best.

Metric	EquiformerV2	Baseline (ET)	CT-SCD	CGT-SCD	JMP-S	JMP-L
Model Parameters	11.2M	7M	10M	17M	27M	235M
Pretraining Structures	0	0	3.4M (U)	3.4M (U)	120M (L)	120M (L)
Pretraining GPU-hours	0	0	298	<u>1,308</u>	5,700	34,400
Finetuning GPU-h/task	137	—	46	<u>96</u>	—	—
Total hours (10 tasks)	<u>1,370</u>	—	758	2,268	> 5,700	> 34,400
QM9 Task (MAE)						
HOMO (meV)	14.0	20.3	12.7	<u>9.65</u>	11.1	8.8
LUMO (meV)	13.0	17.5	11.5	<u>9.05</u>	10.8	8.6
Gap (meV)	29.0	36.1	24.5	<u>19.7</u>	23.1	19.1
ZPVE (meV)	1.47	1.84	1.18	1.22	<u>1.0</u>	0.9
α (a_0^3)	0.050	0.059	0.0377	0.0383	<u>0.037</u>	0.032
C_v (cal/mol K)	0.023	0.026	0.021	0.019	<u>0.018</u>	0.017
U_0 (meV)	6.17	6.15	3.58	3.96	<u>3.3</u>	2.9
U (meV)	6.49	6.38	3.50	4.11	<u>3.3</u>	2.8
H (meV)	6.22	6.16	3.52	4.00	<u>3.3</u>	2.8
G (meV)	7.57	7.62	5.29	5.29	<u>4.5</u>	4.3

(U) denotes unlabeled geometries; (L) denotes labeled force-energy structures.

Table 6. Matbench Bandgap Prediction. SCD models achieve competitive performance with significantly fewer parameters and unlabeled structures. Within each category best results are **bolded**; second best are underlined.

Model	MAE (eV)	Params	Data
No Pretraining			
coGN (Ruff et al., 2023)	0.156	—	n/a
CT (Baseline)	<u>0.186</u> [†]	10M	n/a
JMP-S (Shoghi et al., 2023)	0.235 [†]	25.2M	n/a
JMP-L (Shoghi et al., 2023)	0.228 [†]	235M	n/a
MODNet (De Breuck et al., 2021)	0.220	—	n/a
FE Pretrained			
JMP-L (Shoghi et al., 2023)	0.091	235M	120M
JMP-S (Shoghi et al., 2023)	<u>0.121</u>	27M	120M
CT-FE-OMOL25	0.134 [†]	10M	4M
HackNIP (Kim et al., 2025)	0.150	> 25M	> 32M*
SCD Pretrained (Ours)			
CT-SCD-AMP20	0.123	10M	675k
CT-SCD-ALL	<u>0.132</u> [†]	10M	11.3M
CT-SCD-OMOL25	0.136 [†]	10M	4M

[†] Reported from Fold 0. See full results in table 12.

* Estimated from Orb-v2 backbone.

ing pretraining GPU-hours. Table 5). Furthermore, large datasets are not always necessary to realize these benefits. Pretraining on a random 10% slice of the PCQ dataset (300k molecules) captures 97% of the performance gain of the full dataset for QM9 tasks, and pretraining on just 607k materials yields band gap accuracies within 1.7% of larger models pretrained on 120M force-energy labeled geometries, 108M of which are from materials. Overall, we find that efficient

Table 7. Ligand binding affinity: RMSE on the 30% (id30) and 60% (id60) sequence identity overlap splits. Best results are **bolded**; second best are underlined.

Model	RMSE: id30 / id60 ↓	Params
No Pretraining		
ProtNet (Wang et al., 2023)	1.463 / 1.343	—
EPT-Scratch (Jiao et al., 2025)	1.378 / 1.277	30M
CT (Baseline)	1.510 / 1.386	10M
Other Pretrained		
Uni-Mol (Zhou et al., 2023)	1.520 / 1.619	47.6M
EPT-Protein (Jiao et al., 2025)	1.329 / 1.235	30M
EPT-Multi (Jiao et al., 2025)	1.322 / 1.227	30M
ADiT-S (Anonymous, 2025)	1.337 / 1.413	12M
ADiT-M (Anonymous, 2025)	1.353 / 1.335	35M
ADiT-L (Anonymous, 2025)	<u>1.308</u> / 1.246	253M
SCD Pretrained (Ours)		
CT-SCD-ALL	1.372 / 1.218	10M
CT-SCD-PCQ	1.332 / 1.226	10M
CT-SCD-SAIR	1.337 / <u>1.196</u>	10M
CT-SCD-SAIR-Pocket	1.304 / 1.200	10M
CT-SCD-OMOL25	1.389 / 1.175	10M

Full results provided in Table 11.

pretraining is more impactful and cost effective than implementing inductive bias through complex architectural elements (as has been found in other fields).

Data relevance is key to performance: Across all tasks explored, the strongest predictor of success was similarity between samples in the pretraining dataset and the fine-tuning dataset. This was most apparent in materials bandgap prediction, in which pretraining datasets containing inorganic atoms provided far greater benefit than those containing

Table 8. **Comparing the Impact of Different Pretraining Data.** Pretraining on any data source benefits every task, though downstream performance gains are greatest when pretraining on in-domain data. Datasets with high elemental diversity yield the highest average improvements. *CT-FE* models denote supervised force-energy pretraining; *CT-SCD* denotes self-supervised pretraining. Best results are **bold**; second best are underlined.

Model (Pretraining Data)	QM9 (Small Mol.)		Matbench (Crystals)		LBA (Proteins)		Avg % imp.
	HOMO (meV)	% imp.	MP Gap (eV)	% imp.	RMSE (id60)	% imp.	
ET/CT (Baseline)	20.3	0.0%	0.186	0.0%	1.386	0.0%	0.0%
CT-SCD-PCQ	12.7	37.4%	0.174	6.5%	1.226	11.5%	18.5%
CT-SCD-GEOM10	<u>13.2</u>	35.0%	0.177	4.8%	1.211	12.6%	17.5%
CT-SCD-AMP20	14.6	28.1%	0.122	34.4%	1.219	12.0%	24.8%
CT-SCD-SAIR	14.6	28.1%	0.182	2.2%	1.196	13.7%	14.6%
CT-SCD-ALL	12.7	37.4%	<u>0.132</u>	29.0%	1.218	12.1%	<u>26.2%</u>
CT-FE-OMol25	13.6	33.0%	0.134	28.0%	<u>1.187</u>	14.4%	25.1%
CT-SCD-OMol25	12.8	36.9%	0.136	26.9%	1.175	15.2%	26.4%

only organic elements. Notably, our model pretrained on a combine super-set of single domain data (CT-SCD-ALL) achieved significantly better average performance across all domains, but did not surpass the performance of copies pretrained on single-domain data for in-domain tasks. We attribute this small drop in performance to the limited expressivity of our 10M parameter model rather than representation conflicts in multi-domain training, though further studies are needed to confirm this. We expect larger models to receive greater benefit from pretraining with large multi-domain datasets.

Pretraining a Foundation Model does not require labels:

Force-energy pretraining has proven to be an effective and scalable pretraining strategy when DFT labels are readily available (Shoghi et al., 2023; Kim et al., 2025). However, computing large numbers of new ground truth (DFT) forces and energies is extremely expensive and time-consuming. Finding effective methods of pretraining with unlabeled, low fidelity, and or cheaply generated atomistic geometries could enable further generalization of atomistic foundation models without requiring a significant expansion of DFT labeled datasets. We provide SCD as a demonstration that this is possible through self-supervised learning. When controlling for architecture and pretraining geometries (labeled vs unlabeled), SCD pretraining can match or surpass the performance of supervised force-energy pretraining in downstream property prediction tasks. Further, we show that even diffusion generated conformers (i.e. SAIR) benefit SCD pretraining. As generative methods in the atomistic sciences continue to advance, we anticipate an increased availability of large ‘synthetic’ datasets for pretraining.

In developing SCD, our aim is to inspire further exploration into self-supervised learning and efficient pretraining for atomistic foundation models. More work is still needed to investigate the effects of scaling across dataset and model dimensions. To assist in this ef-

fort, we’ve made our code and pre-trained models publicly available at <https://github.com/TyJPerez/SelfConditionedDenoisingAtoms>

Acknowledgements

We thank Kaiming He and Bowen Deng for valuable feedback and helpful discussions on this work. This research used resources of the National Energy Research Scientific Computing Center (NERSC), a Department of Energy User Facility using NERSC award ALCC-ERCAP 0038200.

Impact Statement

This paper aims to advance applications of Machine Learning in the atomistic sciences. Specifically, we focus on improving the efficacy of self-supervised pretraining, potentially reducing the need for computationally expensive DFT labels. Any societal consequences or impacts that typically relate to the development of atomistic foundation models also apply here. Foundation models and their derivative tools could lower the cost of discovery in many areas of science, including dual use technologies.

References

- Anonymous. Towards all-atom foundation models for biomolecular binding affinity prediction. In *Submitted to The Fourteenth International Conference on Learning Representations*, 2025. URL <https://openreview.net/forum?id=o0Qfsq1fk8>. under review.
- Axelrod, S. and Gomez-Bombarelli, R. Geom: Energy-annotated molecular conformations for property prediction and molecular generation, 2022. URL <https://arxiv.org/abs/2006.05531>.
- Batatia, I., Benner, P., Chiang, Y., Elena, A. M., Kovács,

- D. P., Riebesell, J., Advincula, X. R., Asta, M., Avaylon, M., Baldwin, W. J., Berger, F., Bernstein, N., Bhowmik, A., Bigi, F., Blau, S. M., Cărare, V., Ceriotti, M., Chong, S., Darby, J. P., De, S., Pia, F. D., Deringer, V. L., Elijošius, R., El-Machachi, Z., Falcioni, F., Fako, E., Ferrari, A. C., Gardner, J. L. A., Gawkowski, M. J., Genreith-Schriever, A., George, J., Goodall, R. E. A., Grandel, J., Grey, C. P., Grigorev, P., Han, S., Handley, W., Heenen, H. H., Hermansson, K., Holm, C., Ho, C. H., Hofmann, S., Jaafar, J., Jakob, K. S., Jung, H., Kapil, V., Kaplan, A. D., Karimitari, N., Kermode, J. R., Kourtis, P., Kroupa, N., Kullgren, J., Kuner, M. C., Kuryla, D., Liepuoniute, G., Lin, C., Margraf, J. T., Magdău, I.-B., Michaelides, A., Moore, J. H., Naik, A. A., Niblett, S. P., Norwood, S. W., O'Neill, N., Ortner, C., Persson, K. A., Reuter, K., Rosen, A. S., Rosset, L. A. M., Schaaf, L. L., Schran, C., Shi, B. X., Sivonxay, E., Stenczel, T. K., Svahn, V., Sutton, C., Swinburne, T. D., Tilly, J., van der Oord, C., Vargas, S., Varga-Umbrich, E., Vegge, T., Vondrák, M., Wang, Y., Witt, W. C., Wolf, T., Zills, F., and Csányi, G. A foundation model for atomistic materials chemistry, 2025. URL <https://arxiv.org/abs/2401.00096>.
- Chen, X., Xie, S., and He, K. An empirical study of training self-supervised vision transformers, 2021. URL <https://arxiv.org/abs/2104.02057>.
- Chmiela, S., Tkatchenko, A., Sauceda, H. E., Poltavsky, I., Schütt, K. T., and Müller, K.-R. Machine learning of accurate energy-conserving molecular force fields. *Science Advances*, 3(5):e1603015, May 2017. doi: 10.1126/sciadv.1603015. URL <https://doi.org/10.1126/sciadv.1603015>.
- De Breuck, P.-P., Hautier, G., and Rignanese, G.-M. Materials property prediction for limited datasets enabled by feature selection and joint learning with modnet. *npj Computational Materials*, 7(83), 2021. doi: 10.1038/s41524-021-00552-2.
- Dunn, A., Wang, Q., Ganose, A., Dopp, D., and Jain, A. Benchmarking materials property prediction methods: the matbench test set and automatminer reference algorithm. *npj Computational Materials*, 6(1):138, 2020. doi: 10.1038/s41524-020-00406-3. URL <https://doi.org/10.1038/s41524-020-00406-3>.
- Fang, A., Zhang, Z., Zhou, A., and Zitnik, M. Atomica: Learning universal representations of intermolecular interactions. *bioRxiv*, pp. 2025–04, 2025.
- Feng, R., Zhu, Q., Tran, H., Chen, B., Toland, A., Ramprasad, R., and Zhang, C. May the force be with you: Unified force-centric pre-training for 3d molecular conformations, 2023. URL <https://arxiv.org/abs/2308.14759>.
- Feng, S., Ni, Y., Li, M., Huang, Y., Ma, Z.-M., Ma, W.-Y., and Lan, Y. Unicorn: A unified contrastive learning approach for multi-view molecular representation learning. *arXiv preprint arXiv:2405.10343*, 2024.
- Gao, B., Jia, Y., Mo, Y., Ni, Y., Ma, W., Ma, Z., and Lan, Y. Profsa: Self-supervised pocket pretraining via protein fragment-surroundings alignment. *arXiv preprint arXiv:2310.07229*, 2023.
- Godwin, J., Schaarschmidt, M., Gaunt, A. L., Sanchez-Gonzalez, A., Rubanova, Y., Veličković, P., Kirkpatrick, J., and Battaglia, P. Simple GNN regularisation for 3d molecular property prediction and beyond. In *International Conference on Learning Representations*, 2022. URL <https://openreview.net/forum?id=1wVvweK3oIb>.
- He, K., Chen, X., Xie, S., Li, Y., Dollár, P., and Girshick, R. Masked autoencoders are scalable vision learners, 2021. URL <https://arxiv.org/abs/2111.06377>.
- Hu, W., Liu, B., Gomes, J., Zitnik, M., Liang, P., Pande, V., and Leskovec, J. Strategies for pre-training graph neural networks, 2020. URL <https://arxiv.org/abs/1905.12265>.
- Jain, A., Ong, S. P., Hautier, G., Chen, W., Richards, W. D., Dacek, S., Cholia, S., Gunter, D., Skinner, D., Ceder, G., et al. Commentary: The materials project: A materials genome approach to accelerating materials innovation. *APL materials*, 1(1), 2013.
- Jiao, R., Kong, X., Zhang, L., Yu, Z., Ren, F., Tan, W., Huang, W., and Liu, Y. An equivariant pretrained transformer for unified 3d molecular representation learning, 2025. URL <https://arxiv.org/abs/2402.12714>.
- Joshi, C. K., Fu, X., Liao, Y.-L., Gharakhanyan, V., Miller, B. K., Sriram, A., and Ulissi, Z. W. All-atom diffusion transformers: Unified generative modelling of molecules and materials. *arXiv preprint arXiv:2503.03965*, 2025.
- Kim, S. Y., Park, Y. J., and Li, J. Leveraging neural network interatomic potentials for a foundation model of chemistry. *arXiv preprint arXiv:2506.18497*, 2025. URL <https://arxiv.org/pdf/2506.18497>.
- Lemos, P., Beckwith, Z., Bandi, S., Van Damme, M., Crivelli-Decker, J., Shields, B. J., Merth, T., Jha, P. K., De Mitri, N., Callahan, T. J., et al. Sair: Enabling deep learning for protein-ligand interactions with a synthetic structural dataset. *bioRxiv*, pp. 2025–06, 2025.
- Levine, D. S., Shuaibi, M., Spotte-Smith, E. W. C., Taylor, M. G., Hasyim, M. R., Michel, K., Batatia, I., Csányi, G., Dzamba, M., Eastman, P., et al. The open molecules

- 2025 (omol25) dataset, evaluations, and models. *arXiv preprint arXiv:2505.08762*, 2025.
- Li, Z., Zhou, C., Wang, X., Peng, X., and Zhang, M. Geometric representation condition improves equivariant molecule generation. *arXiv preprint arXiv:2410.03655*, 2024.
- Liao, Y. and Smidt, T. Equiformer: Equivariant graph attention transformer for 3d atomistic graphs. *arXiv preprint arXiv:2206.11990*, 2022. doi: 10.48550/arXiv.2206.11990. URL <https://arxiv.org/abs/2206.11990>.
- Liao, Y., Smidt, T., Wood, B., and Das, A. Equiformerv2: Improved equivariant transformer for scaling to higher-degree representations. *arXiv preprint arXiv:2306.12059*, 2023. doi: 10.48550/arXiv.2306.12059. URL <https://arxiv.org/abs/2306.12059>.
- Liao, Y.-L., Smidt, T., Shuaibi, M., and Das, A. Generalizing denoising to non-equilibrium structures improves equivariant force fields, 2024. URL <https://arxiv.org/abs/2403.09549>.
- Liu, S., Wang, H., Liu, W., Lasenby, J., Guo, H., and Tang, J. Pre-training molecular graph representation with 3d geometry, 2022. URL <https://arxiv.org/abs/2110.07728>.
- Liu, S., Guo, H., and Tang, J. Molecular geometry pre-training with se(3)-invariant denoising distance matching, 2023. URL <https://arxiv.org/abs/2206.13602>.
- Magar, R., Wang, Y., and Barati Farimani, A. Crystal twins: self-supervised learning for crystalline material property prediction. *npj Computational Materials*, 8(1):231, 2022. ISSN 2057-3960. doi: 10.1038/s41524-022-00921-5. URL <https://doi.org/10.1038/s41524-022-00921-5>.
- Nakata, M. and Shimazaki, T. Pubchemqc project: A large-scale first-principles electronic structure database for data-driven chemistry. *Journal of Chemical Information and Modeling*, 57(6):1300–1308, 2017. ISSN 1549-9596. doi: 10.1021/acs.jcim.7b00083. URL <https://doi.org/10.1021/acs.jcim.7b00083>.
- Ni, Y., Feng, S., Ma, W.-Y., Ma, Z.-M., and Lan, Y. Sliced denoising: A physics-informed molecular pre-training method. *arXiv preprint arXiv:2311.02124*, 2023.
- Ni, Y., Feng, S., Hong, X., Sun, Y., Ma, W.-Y., Ma, Z.-M., Ye, Q., and Lan, Y. Pre-training with fractional denoising to enhance molecular property prediction. *Nature Machine Intelligence*, 2024. doi: 10.1038/s42256-024-00900-z. URL <https://www.nature.com/articles/s42256-024-00900-z>.
- Oquab, M., Darcet, T., Moutakanni, T., Vo, H., Szafraniec, M., Khalidov, V., Fernandez, P., Haziza, D., Massa, F., El-Nouby, A., Assran, M., Ballas, N., Galuba, W., Howes, R., Huang, P.-Y., Li, S.-W., Misra, I., Rabbat, M., Sharma, V., Synnaeve, G., Xu, H., Jegou, H., Mairal, J., Labatut, P., Joulin, A., and Bojanowski, P. Dinov2: Learning robust visual features without supervision, 2024. URL <https://arxiv.org/abs/2304.07193>.
- Passaro, S., Corso, G., Wohlwend, J., Reveiz, M., Thaler, S., Somnath, V. R., Getz, N., Portnoi, T., Roy, J., Stark, H., et al. Boltz-2: Towards accurate and efficient binding affinity prediction. *BioRxiv*, 2025.
- Peebles, W. and Xie, S. Scalable diffusion models with transformers, 2023. URL <https://arxiv.org/abs/2212.09748>.
- Ramakrishnan, R., Dral, P. O., Rupp, M., and von Lilienfeld, O. A. Quantum chemistry structures and properties of 134 kilo molecules. *Scientific Data*, 1:140022, 2014. doi: 10.1038/sdata.2014.22. URL <https://doi.org/10.1038/sdata.2014.22>.
- Rhodes, B., Vandenhaute, S., Šimkus, V., Gin, J., Godwin, J., Duignan, T., and Neumann, M. Orb-v3: atomistic simulation at scale, 2025. URL <https://arxiv.org/abs/2504.06231>.
- Ruff, R., Reiser, P., Stühmer, J., and Friederich, P. Connectivity optimized nested graph networks for crystal structures, 2023. URL <https://arxiv.org/abs/2302.14102>.
- Schmidt, J., Wang, H., Cerqueira, T. F. T., Botti, S., and Marques, M. A. L. A dataset of 175k stable and metastable materials calculated with the PBEsol and SCAN functionals. *Scientific Data*, 9(1):64, 2022. ISSN 2052-4463. doi: 10.1038/s41597-022-01177-w. URL <https://doi.org/10.1038/s41597-022-01177-w>.
- Schmidt, J., Hoffmann, N., Wang, H.-C., Borlido, P., Carriço, P. J. M. A., Cerqueira, T. F. T., Botti, S., and Marques, M. A. L. Machine-learning-assisted determination of the global zero-temperature phase diagram of materials. *Advanced Materials*, 35(22):2210788, 2023. doi: <https://doi.org/10.1002/adma.202210788>. URL <https://advanced.onlinelibrary.wiley.com/doi/abs/10.1002/adma.202210788>.
- Shoghi, N., Kolluru, A., Kitchin, J. R., Ulissi, Z. W., Zitnick, C. L., and Wood, B. M. From molecules to materials: Pre-training large generalizable models for atomic property prediction. *arXiv preprint arXiv:2310.16802*, 2023.
- Siméoni, O., Vo, H. V., Seitzer, M., Baldassarre, F., Oquab, M., Jose, C., Khalidov, V., Szafraniec, M., Yi, S., Ramamonjisoa, M., Massa, F., Haziza, D., Wehrstedt, L., Wang,

- J., Darcet, T., Moutakanni, T., Sentana, L., Roberts, C., Vedaldi, A., Tolan, J., Brandt, J., Couprie, C., Mairal, J., Jégou, H., Labatut, P., and Bojanowski, P. Dinov3, 2025. URL <https://arxiv.org/abs/2508.10104>.
- Somnath, V. R., Bunne, C., and Krause, A. Multi-scale representation learning on proteins. *Advances in Neural Information Processing Systems*, 34:25244–25255, 2021.
- Stärk, H., Beaini, D., Corso, G., Tossou, P., Dallago, C., Günnemann, S., and Liò, P. 3d infomax improves gnns for molecular property prediction, 2022. URL <https://arxiv.org/abs/2110.04126>.
- Thölke, P. and Fabritiis, G. D. Torchmd-net: Equivariant transformers for neural network based molecular potentials, 2022. URL <https://arxiv.org/abs/2202.02541>.
- Tomasev, N., Bica, I., McWilliams, B., Buesing, L., Pascanu, R., Blundell, C., and Mitrovic, J. Pushing the limits of self-supervised resnets: Can we outperform supervised learning without labels on imagenet?, 2022. URL <https://arxiv.org/abs/2201.05119>.
- Townshend, R. J. L., Vögele, M., Suriana, P., Derry, A., Powers, A., Laloudakis, Y., Balachandar, S., Jing, B., Anderson, B., Eismann, S., Kondor, R., Altman, R. B., and Dror, R. O. Atom3d: Tasks on molecules in three dimensions, 2022. URL <https://arxiv.org/abs/2012.04035>.
- Wang, L., Liu, H., Liu, Y., Kurtin, J., and Ji, S. Learning hierarchical protein representations via complete 3d graph networks, 2023. URL <https://arxiv.org/abs/2207.12600>.
- Wohlwend, J., Corso, G., Passaro, S., Getz, N., Reveiz, M., Leidal, K., Swiderski, W., Atkinson, L., Portnoi, T., Chinn, I., et al. Boltz-1 democratizing biomolecular interaction modeling. *BioRxiv*, pp. 2024–11, 2025.
- Wood, B. M., Dzamba, M., Fu, X., Gao, M., Shuaibi, M., Barroso-Luque, L., Abdelmaqsoud, K., Gharakhanyan, V., Kitchin, J. R., Levine, D. S., Michel, K., Sriram, A., Cohen, T., Das, A., Rizvi, A., Sahoo, S. J., Ulissi, Z. W., and Zitnick, C. L. Uma: A family of universal models for atoms, 2025. URL <https://arxiv.org/abs/2506.23971>.
- Wu, F., Tao, Y., Radev, D., and Xu, J. When geometric deep learning meets pretrained protein language models. *bioRxiv*, pp. 2023–01, 2023.
- Yuan, E. C. Y., Liu, Y., Chen, J., Zhong, P., Raja, S., Kreiman, T., Vargas, S., Xu, W., Head-Gordon, M., Yang, C., Blau, S. M., Cheng, B., Krishnapriyan, A., and Head-Gordon, T. Foundation models for atomistic simulation of chemistry and materials, 2025. URL <https://arxiv.org/abs/2503.10538>.
- Zaidi, S. Response to issue #3 on *shehzaidi/pre-training-via-denoising*: Training stability for homo/lumo tasks. <https://github.com/shehzaidi/pre-training-via-denoising/issues/3#issuecomment-1670261990>, 2023. GitHub issue comment.
- Zaidi, S., Schaarschmidt, M., Martens, J., Kim, H., Teh, Y. W., Sanchez-Gonzalez, A., Battaglia, P., Pascanu, R., and Godwin, J. Pre-training via denoising for molecular property prediction. *arXiv preprint arXiv:2206.00133*, 2022.
- Zeni, C., Pinsler, R., Zügner, D., Fowler, A., Horton, M., Fu, X., Shysheya, S., Crabbé, J., Sun, L., Smith, J., et al. Mattergen: a generative model for inorganic materials design. *arXiv preprint arXiv:2312.03687*, 2023.
- Zhang, X., Wang, L., Helwig, J., Luo, Y., Fu, C., Xie, Y., Liu, M., Lin, Y., Xu, Z., Yan, K., et al. Artificial intelligence for science in quantum, atomistic, and continuum systems. *Foundations and Trends® in Machine Learning*, 18(4):385–912, 2025.
- Zhou, G., Gao, Z., Ding, Q., Zheng, H., Xu, H., Wei, Z., Zhang, L., and Ke, G. Uni-mol: A universal 3d molecular representation learning framework. In *The Eleventh International Conference on Learning Representations*, 2023. URL <https://openreview.net/forum?id=6K2RM6wVqKu>.

A. Practical Notes on Node Denoising

A.1. Interpreting Noise Scales

We find that the scale of noise applied to atomistic structures plays a significant role in its utility as a pretraining or regularization tool. Here we formalize two distinct regimes:

Regularizing noise utilizes a small scale with respect to bond length (single bonds range from ~ 1.0 to 2.0\AA), such as $\sigma \approx 0.005\text{\AA}$, in order to reduce overfitting. At this scale gaussian noise does not alter single-double bond distinguishability, and is often used as an auxiliary task (Godwin et al., 2022; Liao & Smidt, 2022; Liao et al., 2023). We find that regularizing noise improves downstream results when used in SCD pretraining (on non-corrupted inputs) and performance during some finetuning tasks, but not all.

Corruption noise used for pretraining, is typically one order of magnitude larger ($\sigma \approx 0.04\text{\AA}$), and often perturbs molecular geometries enough to disrupt single/double/triple bond identities ($\pm 0.1\text{\AA}$), but without moving atoms far enough to be considered bond breaking. We find that noise scales much larger than this harm pretraining performance.

A.2. Reinterpreting Denoising for Atomistic Systems

Many previous works have suggested a relationship between denoising objectives and learning ‘force fields’; however, we do not find this to be a useful hypothesis for why denoising benefits representation. It is often implied that the ‘field’ learned by noise prediction is beneficial due to its similarity to DFT forces, yet prior work has shown that noise vectors on ground-state geometries correlate poorly with true DFT forces (Ni et al., 2023). Consistent with this, we find that for our models trained on ground-truth DFT forces, adding an auxiliary node denoising objective harms performance on property prediction, suggesting a low similarity between these targets (see Table 14).

Instead, we hypothesize that denoising objectives succeed because they encourage the development of smooth, distinguishable local atom embeddings. SCD complements this by introducing a global semantic objective. Through this lens, we attribute the transferability of force-energy pretraining to its demand for high geometric sensitivity and representational complexity, rather than to its explicit connection to physical principles. Force prediction encourages equivariant sensitivity to local perturbations, while energy prediction promotes global representation. Based on this hypothesis, we suggest that self-supervised learning methods should employ reconstruction or de-corruption objectives that challenge models with both local and global objectives similar to force-energy pretraining and SCD.

B. Backbone Architecture and Implementation

Self-Conditioned Denoising pretraining can be implemented with any architecture designed for diffusion. To modify an existing non-conditional GNN for SCD pretraining, we replace the pre-norm of each message passing layer with an adaptive layer norm (AdaNorm), similar to a diffusion transformer (Peebles & Xie, 2023).

Figure 3 diagrams our implementation of AdaNorm used for SCD. Because SCD pretraining requires two forward passes per-step we find that including drop path with a drop probability of 0.1 improves training stability and provides an additional form of regularization. Our drop path is implemented to jointly drop both L0 and L1 embeddings. During pretraining we also freeze atom type/element embeddings. Without freezing element embeddings, we find that element embeddings become vanishingly small, leading to downstream instability. On github (Zaidi, 2023), previous authors have noted challenges (gradient explosion) during the downstream fine tuning of models trained by standard node-denoising pretraining (aka ‘coord’) - likely a result of small or zeroed out embedding vectors.

Table 9 shows a breakdown of parameter count, speed, and memory usage for the architectures used in this work. Each architecture shown uses the same embedding size (256), number of layers (8), and number of attention heads (8). CT and CGT correspond to the modified architectures of ET and GET that incorporate conditional layer norms. In this table, we can see that adding conditional guidance to an architecture has little effect on its speed and memory usage as compared to the addition of edge updates and angle embeddings. CT is overall 4 times faster, almost half the size, and has half the peak memory usage as GET.

Table 9. **Architecture Efficiency Comparison.** Benchmarked using QM9 molecules, with batch size 128, averaged over 32 batches, on a NVIDIA RTX A5000 GPU. All models share identical embedding dimensions, layer counts, and attention heads. Parameter counts in this table encompass only backbone architecture, excluding the embedding and prediction heads. All metrics shown are computed from singular forward passes.

(a) **Absolute Metrics:** Latency (lower is better), Throughput (higher is better), and Memory.

Model	Params (M)	Latency (ms) ↓		Throughput (samp/s) ↑		Avg Mem (GB)		Peak Mem (GB)	
		Eval	Train	Eval	Train	Eval	Train	Eval	Train
ET	6.5	65.7	69.1	1946	880	0.04	0.13	1.07	8.47
CT	9.2	70.6	74.5	1812	802	0.05	0.15	1.08	9.00
GET	13.4	264.9	369.5	483	194	0.07	0.18	1.62	20.37
CGT	16.0	262.8	379.3	487	189	0.08	0.20	1.63	20.72

(b) **Relative Metrics:** Normalized to ET baseline (1.0×).

Model	Param Ratio	Rel. Speed ↑		Rel. Avg Mem ↓	
		Eval	Train	Eval	Train
ET	1.00×	1.00×	1.00×	1.00×	1.00×
CT	1.40×	0.92×	0.93×	1.25×	1.15×
GET	2.00×	0.25×	0.19×	1.67×	1.38×
CGT	2.45×	0.25×	0.18×	1.90×	1.53×

Table 10. Backbone architecture hyperparameters used in this work. CT-small is only used in the MD17 benchmark

Hyperparameter	CT	CGT	CT-small
Layers	8	8	6
Attention heads	8	8	8
Embedding dimension	256	256	128
Layer pooling	sum	sum	sum
Graph cutoff (Å)	5	5	5
L0 head pooling	sum	sum	sum

C. Supplementary Results

C.1. Ligand Binding Affinity

C.1.1. CONDITIONAL DENOISING OF COUPLED COMPONENTS: POCKETS AND LIGANDS

When dataset samples (\mathbf{x}) contain interdependent pairs ($\mathbf{x} = A \cup B$), such as a protein pocket and a bound ligand, we can alter the self-conditioned denoising objective to instead denoise one component based on an embedding from the other (eqn 4). In doing so we can exploit known conditional relationships in the dataset during pretraining.

$$\mathbb{E}_{q_{\sigma}(\tilde{\mathbf{x}}, \mathbf{x})} \left[\left\| \phi_{\theta}(\tilde{\mathbf{x}} | \mathbf{c}) - \varepsilon \right\|_2^2 \right] = \mathbb{E}_{q_{\sigma}(\tilde{\mathbf{A}}, \mathbf{B})} \left[\left\| \phi_{\theta}(\tilde{\mathbf{A}} | \phi_{\theta}(\mathbf{B})_{L0})_{L1} - \varepsilon_A \right\|_2^2 \right] \quad (4)$$

In table 11 we present results from three variations of pretraining on SAIR. In CT-SCD-SAIR, we pretrain the model using canonical SCD, embedding and denoising the entire pocket-ligand complexes together. However, in pretraining CT-SCD-SAIR-Lig the ligand structure is embedded and used to conditionally denoise the pocket atoms; and in CT-SCD-SAIR-Pocket we do the reverse, pocket atoms are embedded and used to conditionally denoise the ligand atoms. In doing this we find that CT-SCD-SAIR-Pocket performs the best (specifically on low sequence overlap), CT-SCD-SAIR the second best, and CT-SCD-SAIR-Lig the worst. This follows biochemical intuition, as we’d expect ligand conformation to be strongly dependent on pocket geometry, but not the other way around. We hold this as an example of how exploiting known conditional relationships can benefit learned representation during pretraining. We suspect that component conditional de-corrupt objectives may also benefit other pairwise tasks.

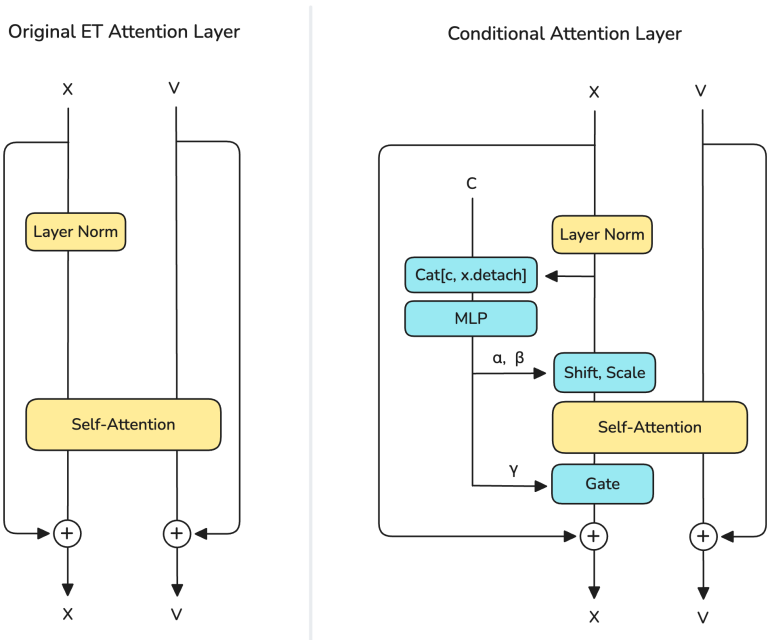


Figure 3. **Adaptive layer normalization for SCD:** On the left we illustrate a simplified diagram of the original residual layer block in TorchMD-Net (ET). Here, 'X' represents invariant (L0) embeddings while 'V' represents equivariant vector embeddings (L1), and 'C' represents the conditioning embedding. On the right, we show how we modify the original residual block with a conditional scale, shift, and gate of the invariant embeddings. In the gate block the gamma vector is attenuated by a tanh function and multiplied to the output of the ET Attention block. For this work, we use a two layer MLP for conditioning in each layer.

C.2. Force-Energy Pretraining and Fine-Tuning For Property Prediction

In this work, we conduct all force-energy pretraining using the OMol25-4M dataset and a CT backbone. In Table 13, we compare models pretrained via either direct ('forward') or gradient-based ('backward' aka 'conservative') force prediction. Unsurprisingly, the simple CT backbone does not yield state-of-the-art force-energy predictions; however, we find that SCD pretraining confers a modest benefit even when restricted to the same training geometries as the labeled task. Additionally, we find that a single SCD step (comprising a double forward pass) is roughly half the speed of a direct force training step (a single forward pass), but $1.4\times$ faster than a gradient-based (forward then 'backwards') force training update step. Table 14 presents benchmarking results for these models on two representative QM9 tasks: HOMO and U_0 (potential energy at 0K). We observe that pretraining via direct force prediction benefits downstream property prediction more than gradient-based force pretraining, but it does not outperform SCD pretraining. In other tables, we report to our best model—pretrained exclusively on direct force prediction—as 'CT-FE-OMOL25'.

C.3. MD17: Small Molecule Forces

Consistent with prior work, we benchmark a smaller SCD model (6 layers, dim 128) on MD17 (Chmiela et al., 2017). The models presented in Table 16 were pre-trained on the PCQ dataset and subsequently fine-tuned on MD17. To match the fine-tuning methods described by Frad (Ni et al., 2024), we also train a model using a two pass 'force-denoise' scheme, in which the first pass is used to predict forces and energies and the second forward pass is used for an auxiliary denoising task. We observe that SCD pre-training with the CT backbone yielded results similar to those of Frad and SLiDe, while achieving $4\times$ faster inference speeds. However, none of these methods achieve particularly strong performance on this benchmark. We hypothesize that this stems from the pre-training dataset containing exclusively ground-state geometries; consequently, the non-equilibrium structures in MD17 are likely out-of-distribution. Lacking non-equilibrium structures during pre-training, the models fail to capture features necessary for non-equilibrium prediction tasks. This aligns with our findings on other benchmarks, where similarity between pre-training and fine-tuning data distributions is a strong predictor of performance. We do not report results for the GET/CGT variant due to persistent numerical instability (segmentation faults) when computing gradient-based forces.

Self-Conditioned Denoising for Atomistic Representation Learning

Table 11. **SCD on Proteins:** Ligand Binding Affinity (LBA) predictions over two sequence identity splits (30% and 60%). SCD models pretrained on synthetic or diverse data (e.g., SAIR, OMol25) can outperform larger models pretrained on PDB-based datasets. Best results within each category are **bolded**; second best are underlined.

Method	Model	Seq. overlap 30%			Seq. overlap 60%			Params
		RMSE ↓	Pear. ↑	Spear. ↑	RMSE ↓	Pear. ↑	Spear. ↑	
No Pretraining	HoloProt-Full Surface (Somnath et al., 2021)	1.464	0.509	0.500	1.365	0.749	0.742	1.4M
	ProtNet-All-Atom (Wang et al., 2023)	1.463	<u>0.551</u>	0.551	<u>1.343</u>	<u>0.765</u>	<u>0.761</u>	—
	ATOM3D-3DCNN (Townshend et al., 2022)	<u>1.416</u>	0.550	<u>0.553</u>	1.621	0.608	0.615	—
	ATOM3D-ENN (Townshend et al., 2022)	1.568	0.389	0.408	1.620	0.623	0.633	—
	ATOM3D-GNN (Townshend et al., 2022)	1.601	0.545	0.533	1.408	0.743	0.743	—
	EPT-Scratch (Jiao et al., 2025)	1.378	0.604	0.594	1.277	0.787	0.785	30M
	CT	1.510	0.501	0.486	1.386	0.736	0.720	10M
Pretrained on PCQ	Frad (Ni et al., 2024)	1.365	0.599	0.577	1.213	0.804	0.801	14M
	CT-SCD-PCQ	1.332	0.617	0.600	1.226	0.800	0.794	10M
Other Pretrained	EGNN-PLM (Wu et al., 2023)	1.403	0.565	0.544	1.559	0.644	0.646	650M
	Uni-Mol (Zhou et al., 2023)	1.520	0.558	0.540	1.619	0.645	0.653	47.6M
	ProFSA (Gao et al., 2023)	1.377	0.628	0.620	1.377	0.764	0.762	47.6M
	EPT-Molecule (Jiao et al., 2025)	1.336	0.621	0.602	1.243	0.802	0.800	30M
	EPT-Protein (Jiao et al., 2025)	1.329	0.628	0.613	<u>1.235</u>	<u>0.804</u>	<u>0.800</u>	30M
	EPT-MultiDomain (Jiao et al., 2025)	<u>1.322</u>	<u>0.644</u>	<u>0.630</u>	1.227	0.811	0.803	30M
	ADiT-S (Anonymous, 2025)	1.337	0.626	0.618	1.413	0.740	0.740	12M
	ADiT-M (Anonymous, 2025)	1.353	0.622	<u>0.630</u>	1.335	0.764	0.752	35M
	ADiT-L (Anonymous, 2025)	1.308	0.645	0.647	1.246	0.767	0.765	253M
SCD Pretrained	CT-SCD-AMP20	1.408	0.584	0.533	1.219	0.803	0.800	10M
	CT-SCD-GEOM10	1.392	0.606	0.554	1.211	0.806	0.801	10M
	CT-SCD-ALL	1.372	0.594	0.578	1.218	0.802	0.798	10M
	CT-SCD-SAIR-Lig	1.412	0.566	0.547	1.283	0.779	0.770	10M
	CT-SCD-SAIR	<u>1.337</u>	<u>0.617</u>	<u>0.599</u>	<u>1.196</u>	<u>0.810</u>	0.802	10M
	CT-SCD-SAIR-Pocket	1.304	0.640	0.624	1.200	0.809	<u>0.806</u>	10M
	CT-SCD-OMOL25	1.389	0.586	0.571	1.175	0.817	0.816	10M
FE Pretrained	CT-FE-OMOL25	1.391	0.575	0.564	1.187	0.814	0.811	10M

D. Datasets

D.1. Pretraining Datasets

PCQ: The PCQM4Mv2 dataset is a curated subsample of the PubChemQC project containing ground state geometries for 3.378M organic small molecule obtained using B3LYP/6-31G* DFT (Nakata & Shimazaki, 2017). This dataset is commonly used for demonstrating self-supervised learning methods, either on its own or as part of a composite dataset. Throughout this work we use ‘PCQ’ to indicate models trained only on this dataset.

GEOM10: The original GEOM dataset contains 36M conformers from ~450k unique molecules generated using GFN2-xTB, a semi-empirical extended tight-binding method (Axelrod & Gomez-Bombarelli, 2022). GEOM is split into three categories: 1) GEOM-drugs, containing conformers of drug like small molecules, 2) GEOM-QM9, conformers of molecules from the qm9 dataset, and 3) GEOM-MoleculeNet, containing conformers from a subsample of molecules in the MoleculeNet benchmark. To avoid overlap with benchmarking datasets we only utilize structures from geom-drug, containing 304k unique molecules, and curate two subsamples: GEOM10, containing up to 10 of the lowest energy conformers from each molecule (2.7M geometries total), and GEOM1 containing only the lowest energy (ground-state) conformer from each molecule (304k geometries).

SAIR: The Structurally Augmented IC50 Repository (SAIR) dataset contains a large number of bound protein-ligand structures generated using the Boltz-1x model (Wohlwend et al., 2025). Five conformers are provided for each structure. Although, the authors of the SAIR reports to have 1,048,857 unique binding pairs totaling in 5.2M conformers, the copy we obtained from huggingface (<https://huggingface.co/datasets/SandboxAQ/SAIR>) contains only 888,104 unique binding pairs and 4.4M conformers.

Alex-MP-20: The Alex-MP-20 dataset comprises 607,673 periodic materials structures with up to 20 atoms (Zeni et al., 2023)

Table 12. **SCD on Periodic Materials:** Matbench band gap prediction performance for SCD and supervised force-energy (FE) pretrained models. Best results within each category are **bolded**; second best are underlined. SCD models achieve competitive performance while utilizing significantly fewer parameters and unlabeled structures.

Category	Model	MP Gap (eV)		# Params	Pretraining Data Size
		Fold 0	Mean (0–4)		
No Pretraining	MODNet (De Breuck et al., 2021)	0.215	0.220	—	n/a
	coGN (Ruff et al., 2023)	0.153	0.156	—	n/a
	JMP-S (Shoghi et al., 2023)	0.235	—	25.2M	n/a
	JMP-L (Shoghi et al., 2023)	0.228	—	235M	n/a
	CT (Baseline)	<u>0.186</u>	—	10M	n/a
FE Pretrained	JMP-L (Shoghi et al., 2023)	0.089	0.091	235M	120M
	JMP-S (Shoghi et al., 2023)	<u>0.119</u>	<u>0.121</u>	27M	120M
	HackNIP (Orb-v2 + MODNet) (Kim et al., 2025)	—	0.150	> 25.2M	> 32M*
	CT-FE-OMOL25	0.134	—	10M	4M
Other SSL	Crystal-Twins (Magar et al., 2022)	—	0.264	—	428k
SCD Pretrained	CT-SCD-AMP20	0.122	0.123	10M	675k
	CT-SCD-ALL	<u>0.132</u>	—	10M	11.3M
	CT-SCD-PCQ	0.174	—	10M	3.4M
	CT-SCD-GEOM10	0.177	—	10M	2.8M
	CT-SCD-SAIR	0.182	—	10M	4.4M
	CT-SCD-OMOL25	0.136	—	10M	4M

*Orb-v2 data size estimated from the sum of force-energy finetuning datasets: MPTraj (1.58M) and Alexandria (30.5M) (Kim et al., 2025).

Table 13. **OMol25 4M Force-Energy Pretraining.** Comparison of supervised force-energy training baselines (FE) against finetuning from SCD pretrained weights (SCD-FE). We compare direct force prediction (Forward) against gradient-based force calculation (Backward). CT-SCD-OMOL25 is pretrained by SCD using the same OMol25 4 geometries.

Model Name	Initialization	Force Method	Val Force MAE (meV/Å)	Val Energy MAE (meV)	num training steps
FE-Fwd	From Scratch	Forward	44.8	648	800k
FE-Fwd-long	From Scratch	Forward	42.6	606	1600k
FE-Bwd	From Scratch	Backward	50.0	618	800k
SCD-FE-Fwd	CT-SCD-OMOL25	Forward	42.9 (+4.2%)	617 (+4.8%)	800k (+800k SCD)
SCD-FE-Bwd	CT-SCD-OMOL25	Backward	41.4 (+17.2%)	665 (-7.6%)	800k (+800k SCD)

derived from both the Materials Project (Jain et al., 2013), and the Alexandria materials database (Schmidt et al., 2023; 2022). Throughout this work, we refer to Alex-MP-20 as ‘AMP20’. When SCD pretraining on AMP20, we apply a unit cell repeat augmentation to simulate larger crystals. Each sample is randomly tiled in one direction with a probability ($p_{\text{cell repeat}}$) of 50%, for up to two repeats. This dataset is also available on huggingface (<https://huggingface.co/datasets/OMatG/Alex-MP-20>).

AllAtoms (ALL): We also pretrain on a combine dataset that includes the entirety of PCQ, GEOM10, SAIR, and AlexMP20, totaling in 5.2M unique structures with 11.3M conformations.

OMol25 4M split: The Open Molecular Dataset 2025 (OMol25) is a large-scale repository of over 100 million quantum chemistry calculations covering 83 million unique molecular systems (Levine et al., 2025). While the full dataset spans the first 83 elements (H–Bi) and systems up to 350 atoms, we utilize the designated ‘4M split’, a randomly sampled subset of approximately 4 million geometries. All labels (forces and energies) were computed at the ω B97M-V/def2-TZVPD level of theory. The 4M subset preserves the broad chemical diversity of the full dataset, containing equilibrium and non-equilibrium structures from four primary domains: small organic molecules, biomolecules (proteins, DNA/RNA from PDB/BioLiP2), metal complexes (transition metals, ligands), and electrolytes. This dataset is available on huggingface (<https://huggingface.co/facebook/OMol25>).

Table 14. **Fine-tuning Force-Energy Pretrained Models.** Force-energy pretrained models performed best when the energy head was reset and regularization noise was turned off during finetuning. Forward (non-conservative) force pretraining, conveyed the best average results on downstream property prediction and is reported as ‘CT-FE-OMOL25’ elsewhere.

Model	Fine-tuning Protocol	HOMO (meV)	U_0 (meV)	avg % impv. over baseline
baseline		20.3	6.15	—
FE-Fwd	Standard	15.9	12.9	-44.0%
FE-Fwd	Reset Head, $\sigma_{\text{reg}} = 0.005$	15.0	10.2	-19.9%
FE-Fwd	Reset Head, $\sigma_{\text{reg}} = 0$	13.6	3.40	38.9%
FE-Fwd-long	Reset Head, $\sigma_{\text{reg}} = 0$	13.7	3.47	38.0%
FE-Bwd	Reset Head, $\sigma_{\text{reg}} = 0$	14.5	3.36	37.0%
CT-SCD-OMol25	Standard	12.8	3.54	39.7%

Table 15. SCD vs. other SSL Methods using different backbones and pretraining data. Models CT and CGT below are both pretrained on the PCQ dataset. Best results are **bolded**; second best are underlined.

QM9 Task	CT (Ours)	CGT (Ours)	EPT-10 (Jiao et al., 2025)	Uni-Corn (Feng et al., 2024)
Params	10M	17M	30M	—
Pretrain Data	3.4M	3.4M	5.9M	15M
HOMO (meV)	<u>12.7</u>	9.65	15.2	13.0
LUMO (meV)	<u>11.5</u>	9.05	13.6	11.9
Gap (meV)	<u>24.5</u>	19.7	29.0	24.9
ZPVE (meV)	<u>1.18</u>	1.22	1.11	1.4
U_0 (meV)	3.58	<u>3.96</u>	5.44	3.99
U (meV)	3.50	4.11	5.54	<u>3.95</u>
H (meV)	3.52	4.00	5.42	<u>3.94</u>
G (meV)	<u>5.29</u>	<u>5.29</u>	6.37	5.09
α (a_0^3)	<u>0.0377</u>	0.0383	0.045	0.036
C_v (cal/mol K)	0.021	0.019	0.020	0.019

The pretraining datasets for EPT-10 and Uni-Corn include the 3.4M PCQ structures used by SCD.

D.2. Benchmarking Datasets and Finetuning Hyperparameters

QM9: The QM9 dataset is a commonly used benchmark for small molecule property prediction on 3D geometries (Ramakrishnan et al., 2014). QM9 comprises a set of small organic molecules containing up to nine heavy atoms (C,N,F,O), or up to 29 atoms total when including hydrogen. All 3D Geometries from QM9 are computed using the B3LYP/6-31G(2df, p) DFT functional and are labeled with a set of 15 quantum mechanical properties including homo-lumo gap, atomization energies, specific heat, polarizability and more. The original dataset contains 134k molecules, however it is now standard practice to use a cleaned version containing 130,831. We obtain our copy from the PyTorch Geometric library. QM9 is typically split randomly: 110,000 for training, 10,000 for validation, and the remaining 10,831 for the test set. We use this convention in our work, however we do not use the validation set for early stopping. We follow the practices described in TorchNet-MD (Thölke & Fabritiis, 2022) and subtract provided references energies from atomization energy targets. All other targets are normalized to a standard gaussian for prediction.

LBA: The Ligand Binding Affinity (LBA) dataset comprises 4,463 co-crystallized 3D structures of protein-ligand complexes derived from PDBbind. Binding affinities targets are experimentally derived and provided as negative log of either inhibition or dissociation constant ($-\log(K)$). Two splits are provided based on sequence overlap between proteins in the training set and test set; in ‘id60’ no protein in the training set has more than a 60% sequence overlap with any protein in the testset. Similarly, in ‘id30’ train-test sequence overlap is limited to 30%. Following ATOM3D preprocessing (Townshend et al., 2022), predictions are made using extracted pocket-ligand complexes.

Matbench: The matbench properties dataset (Dunn et al., 2020) provides 13 different tasks (regression and classification) for periodic materials structures to benchmark property prediction models. Across these tasks, training set size ranges from 312-132k samples, each of which are split into 5 folds with predefined test splits. In this work we explore only one regression task, ‘mp_gap’ or bandgap energy prediction, as a proof of concept. We choose bandgap energy because of its

Table 16. SCD achieves comparable performance on MD17 force–energy prediction to prior methods while using a smaller and faster architecture. Best results are in **bold**, second best are underlined.

Method	Baseline	Coord	SCD	SCD (force-denoise)	Frad (force-denoise)	SliDe
Architecture	ET-small	ET-small	CT-small	CT-small	GET-small	GET-small
Pretraining dataset	none	PCQ	PCQ	PCQ	PCQ	PCQ
Forces MAE (kcal/mol/Å)						
Aspirin	0.253	0.211	0.210	<u>0.200</u>	0.209	0.174
Benzene	0.196	0.169	0.171	0.175	0.199	0.169
Ethanol	0.109	0.096	0.120	0.116	<u>0.091</u>	0.088
Malonaldehyde	0.169	0.139	0.186	0.173	0.142	0.154
Naphthalene	0.061	0.053	<u>0.041</u>	0.040	0.053	0.048
Salicylic acid	0.129	0.109	<u>0.101</u>	0.099	0.108	<u>0.101</u>
Toluene	0.067	0.058	<u>0.053</u>	0.051	0.054	0.054
Uracil	0.095	0.074	0.077	0.072	<u>0.076</u>	0.083
Energy MAE (kcal/mol)						
Aspirin	0.123	–	0.0742	0.0705	–	–
Benzene	0.058	–	0.0274	0.0211	–	–
Ethanol	0.052	–	0.0286	0.0280	–	–
Malonaldehyde	0.077	–	0.0432	0.0417	–	–
Naphthalene	0.085	–	0.0163	0.0156	–	–
Salicylic acid	0.093	–	0.0286	0.0290	–	–
Toluene	0.074	–	0.0181	0.0184	–	–
Uracil	0.090	–	0.0190	0.0193	–	–

CGT results on MD17 are omitted due to an unresolved segmentation fault during backpropagation.

economic relevance. The ‘mp_gap’ task provides 106k periodic crystal structures in total, resulting in training set sizes of 84k and test set sizes of 21k. We report results for split 0 with all models tested. For our best model we also report the average of all splits.

MD17: The MD17 (Chmiela et al., 2017) dataset comprises a collection of ab initio molecular dynamics (AIMD) trajectories for eight small organic molecules with DFT forces and energies, commonly used to evaluate MLIPs. Following past convention we use a random split of 950 samples for training, 50 for validation (however we do not employ early stopping), and the remainder as the test set. The total number of geometries provided for each trajectory varies from 150k-1M. All force predictions provided are derived from energy gradients (a backwards pass).

E. Hyperparameters

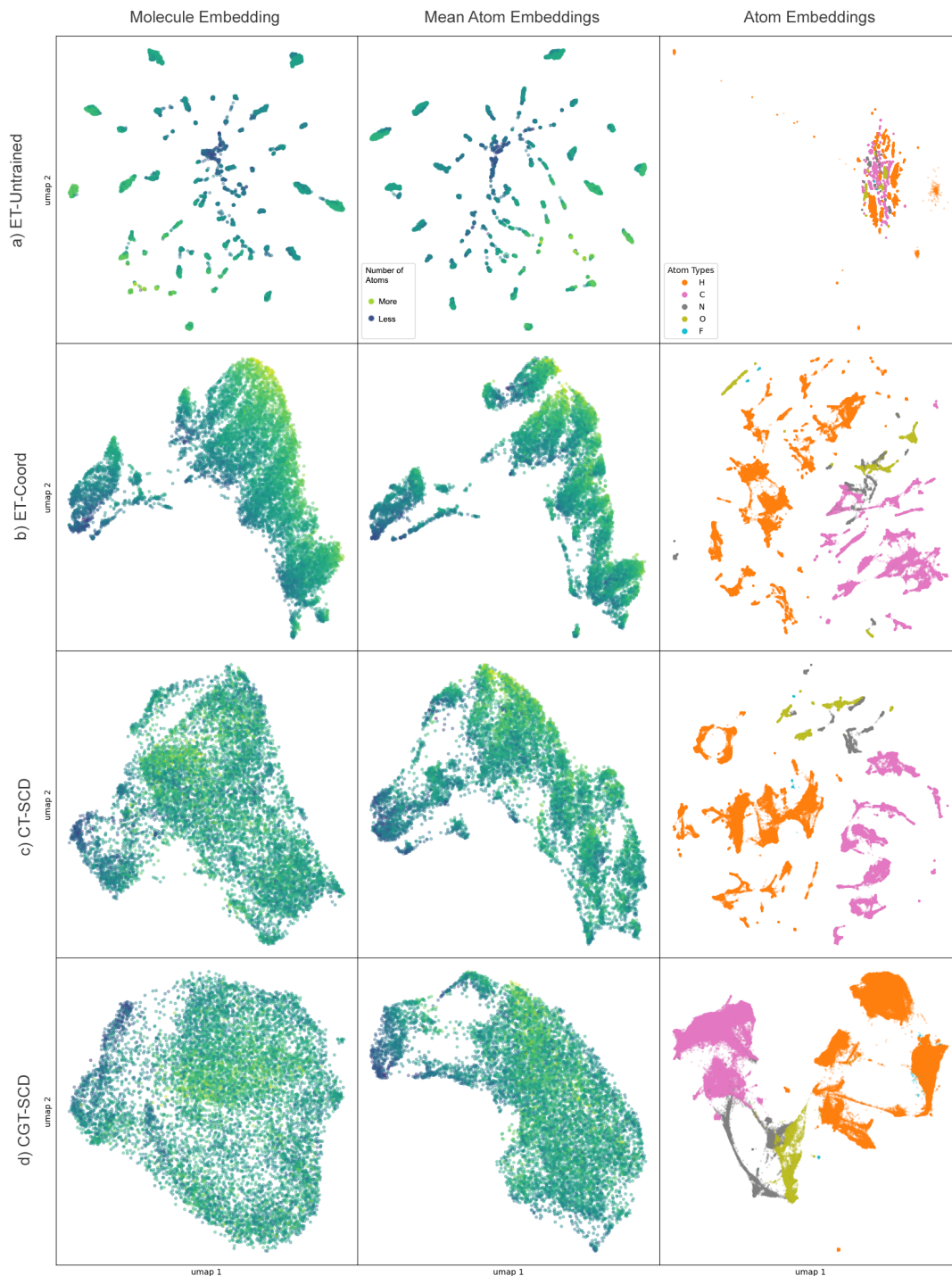


Figure 4. Pretraining Effects on the Embedding Space. UMAP visualizations of embeddings for 10k QM9 molecules, colored by atom count (N). (a) Untrained GNNs exhibit a strong bias towards "extensive" representations, clustering molecules primarily by size (N). (b) Standard node denoising smooths the latent manifold but embeddings remain highly extensive. (c–d) SCD pretraining yields a smoother, less extensive (more semantic) embedding space. We observe that downstream performance improves as representations become smoother and less extensive (Performance: $a < b < c < d$). 'Molecule embeddings' are created by passing sum pooled atom embeddings through a two-layer MLP 'embedding head'. In the case of 'ET-Coord' the embedding head is untrained. In SCD 'Molecule embeddings' are used for self-embeddings. In our 'coord' model, the molecule 'embedding head' remains untrained.

Self-Conditioned Denoising for Atomistic Representation Learning

Table 17. Base SCD pretraining hyperparameters: applied in all SCD training runs

Hyperparameter	Value
Warmup steps	10,000
Learning rate	0.005
β_1	0.9
Weight decay	0.05
DropPath	0.1
Corrupt noise σ	0.04
Regularization noise σ	0.005

Table 18. SCD Pretraining: dataset and model specific hyperparameters.

Backbone	CT	CGT	CT	CT	CT	CT	CT
Dataset	PCQ	PCQ	GEOM10	AMP20	SAIR	ALL	Omol25
Total steps	800k	800k	800k	800k	800k	1.2M	800k
Batch size / GPU	128	32	48	142	12	54	48
# GPUs (A100)	4	16	16	4	8	16	16
Effective batch size	512	512	768	568	96	864	768
Materials augmentations							
Cell repeat iters	–	–	–	2	–	2	–
$p_{\text{cell repeat}}$	–	–	–	0.5	–	0.5	–

E.1. Constants across all training runs

All training runs discussed in this work use the AdamW optimizer with $\beta_2=0.999$, and a learning rate scheduler composed of a linear warm up, followed by cosine decay. No validation sets are used for early stopping, as is often done in other works. All graph creation uses a cutoff distance of 5.0 Å.

Table 19. QM9 finetuning hyperparameters for different target groups.

Hyperparameter	HOMO, LUMO, Gap	U0, U, H, G	Alpha, ZPVE, CV
Batch size	128	32	128
Learning rate	5e-4	3e-4	3e-4
Total steps	300k	500k	400k
Warmup steps	10k	10k	10k
β_1	0.995	0.995	0.95
Weight decay	0.01	0.01	0.01
DropPath (init / final)	0.15 / 0.1	0.15 / 0.0	0.15 / 0.01
Reg. noise σ	0.005	0.0	0.005
Denoise loss weight	0.1	0.0	0.2
Subtract ref. energy	No	Yes	No
Loss EMA	Off	0.05	Off
Head aggregation	Sum	Sum	Sum

Table 20. Matbench finetuning hyperparameters for the mp_gap task.

Hyperparameter	Value
Batch size	8
Learning rate (from scratch)	2e-4
Learning rate (finetuning)	8e-5
Total steps	300k
Warmup steps	10k
β_1	0.995
Weight decay	0.01
DropPath (init / final)	0.15 / 0.00
Reg. noise σ	5e-4
Denoise loss weight	0.01
Head aggregation	Sum

Table 21. Finetuning hyperparameters for the Ligand Binding Affinity (LBA) benchmark

Hyperparameter	Value
Batch size	8
Learning rate (from scratch)	2e-4
Learning rate (finetuning)	1e-4
Total steps	30k
Warmup steps	500
β_1	0.995
Weight decay	0.05
DropPath	0.15
Reg. noise σ	0.005
Denoise loss weight	0.1
Head aggregation	Mean

Table 22. Training hyperparameters for the MD17 benchmark.

Hyperparameter	Value
Backbone	CT-small
Training set size	1,000
Batch size	8
Energy loss EMA	0.05
Energy loss weight	0.8
Force loss weight	0.2
Learning rate	5e-4
Warmup steps	5k
Total steps	150k
β_1	0.995
Weight decay	0.01
DropPath (init / final)	0.15 / 0.00
Reg. noise σ	0.005
Denoise loss weight	0.1
Head aggregation	Sum